Re-engineering potential energy surfaces: trapezoidally distorted $_{\pi}2_{s} + {}_{\pi}2_{s}$ thermal cycloaddition/elimination reactions

Carlota Conesa and Henry S. Rzepa *

Department of Chemistry, Imperial College of Science, Technology and Medicine, South Kensington, London, UK SW7 2AY

Received (in Cambridge) 21st July 1998, Accepted 23rd October 1998

Calculations at the PM3 or B3LYP/6-31G(d) SCF-MO levels of theory indicate that electron-withdrawing substituents can modify the potential energy surface for a simple thermal $_{\pi}2_{s} + {}_{\pi}2_{s}$ pericyclic cycloaddition–elimination *via* a trapezoidal geometric distortion. We propose this thermally allowed synchronous reaction mode as an alternative to the Woodward–Hoffmann antarafacial mode or the stepwise biradical pathways normally invoked for such thermally activated cycloadditions. Reaction of the substituted *syn* tricyclic system **1** *via* the trapezoidal and synchronous transition state **6** is predicted as a potential experimental test of this new reaction mode.

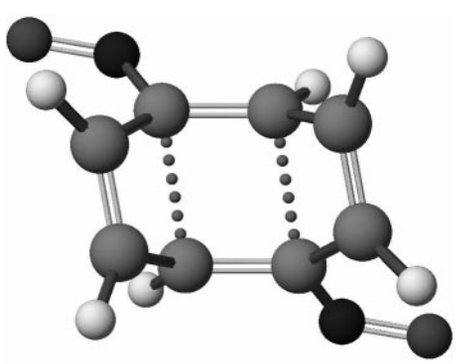

In a previous article[1] we reported possible computed mechanistic pathways for the pericyclic thermal transformation of the *syn* isomers **1** to **5** and the *anti* isomers **7** to **11** (Scheme 1, R = H). These pathways involve either a sequence of transition states and intermediates *via* **3** or **9** (the closed shell stepwise route) or a pathway involving only putative transition states **6** or **12** (the synchronous route). Our motivation was to look at properties such as ring strain in intermediates and aromaticity in transition states that might affect the balance between stepwise and synchronous routes and hence the fundamental nature of the potential energy surface. We were indeed able to locate genuine stationary points on the ground state (thermal) potential energy surfaces for structures **6** and **12**. These are unusual in that they can be regarded either as representing two symmetry allowed conrotatory 4π electrocyclic openings occurring synchronously, or as a single $_{\pi}2_{s} + {}_{\pi}2_{s}$ cycloelimination process. The latter, according to the conventional Woodward–Hoffmann interpretation, must be a thermally forbidden pericyclic process. In the event, both **6** and **12** proved to be second order saddle points, having two imaginary normal

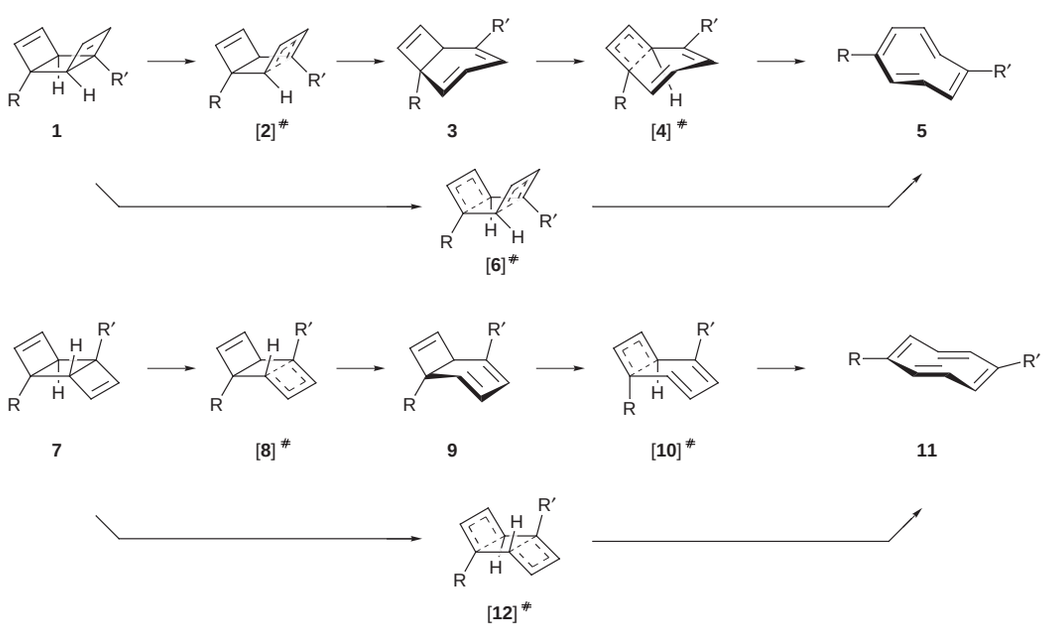

Scheme 1 R = R′ = (**a**) NO_2; (**b**) NO; (**c**) CHO; (**d**) CHS; (**e**) CF; (**f**) CF_3.

modes deriving from the computed Hessian matrix. Whilst the smaller of these negative force constants corresponded to an asymmetric distortion leading the potential surface towards the stepwise pathways *via* **3** and **9**, the more negative force constant did reveal a normal mode which indeed had the apparent form of a $_{\pi}2_{s} + _{\pi}2_{s}$ cycloaddition–elimination process. Although the computed energies of **6** and **12** were higher than any point along the corresponding stepwise pathways, that of **6** in particular was only 10 kcal mol^{-1} higher than the asymmetrically distorted genuine transition state **2**. This unexpectedly low value encouraged us to investigate what effect modification of the potential energy surface with suitable substituents might have. The objectives were to see if (a) **6** or **12** could be converted from a second order to a first order genuine transition state and (b) whether the energies of these particular stationary points could be reduced to below those of **2** or **8**. We report here an investigation of the effect of re-engineering the potential surface using specific pairs of electron withdrawing substituents located at the positions indicated by the R, R′ groups in Scheme 1.

Computational procedure

Approximate geometries were initially optimised at the PM3 level using the MOPAC V6.0 program[2] implemented on CAChe workstations. The transition state structures were located by using an eigenvector following routine (TS) and higher order saddle points were located by minimizing the sum of the squared gradients (NLLSQ). This procedure was followed by calculation of the force constant matrix and normal coordinate analysis to characterize the stationary point, and an intrinsic reaction coordinate calculation along the first normal mode direction to verify the identity of the reactants and products deriving from the transition state for selected examples. Final values of the gradient norms were <0.01 kcal mol^{-1}. Å^{-1}. *Ab initio* calculations were performed starting at PM3 geometries using the GAUSSIAN94 program system,[3] transition states being located by using the Berny algorithm[4] or the synchronous transit-guided quasi-Newton (STQN) methods implemented by Schlegel.[5] Molecular coordinates in the form of Gaussian or Mopac input files for located stationary points are integrated into this article in an enhanced on-line form, together with animations of all important imaginary modes showing the form of the eigenvectors, at the following URL: http://www.rsc.org/suppdata/perkin2/1998/2695.

Results and discussion

Initial studies using the rapid PM3 method led us to focus on the R and R′ positions as the most sensitive location for substituents. Initially, difunctionalisation with the electron push-pull substituents R = CHO, R′ = NH_2 was studied, but this resulted in little energy stabilisation relative to the unsubstituted systems. The stationary points that were located revealed three imaginary frequencies for both possible geometric isomers; **6:** ΔH_{PM3} = 137.08 kcal mol^{-1}, ν = 1054.0i, 952.6i, 325.3i cm^{-1}; **6′**: ΔH_{PM3} = 134.20 kcal mol^{-1}, ν = 902.6i, 617.3i, 490.5i cm^{-1}.

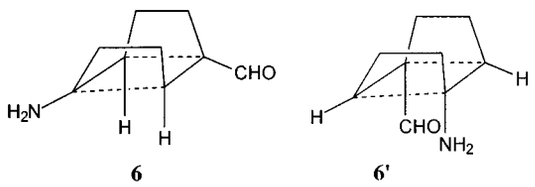

6 **6'**

A significant difference was observed when both R and R′ were selected to be electron-withdrawing groups. In this case, the computed barriers to reaction decrease significantly and all the studied structures **6a**–**f** were now found to be genuine transition states at the PM3 level. In each case, only isomer **6** rather than **6′** could be located. The form of the now single imaginary vibrational mode most resembles a $_{\pi}2_{s} + _{\pi}2_{s}$ cycloelimination rather than two synchronous conrotatory ring openings, but with a distinct trapezoidal component to the geometry (Fig. 1) which still clearly corresponds to suprafacial bond cleavage/formation across the two alkene components. This induced trapezoidal mode is the principal geometric feature which allows the reaction to access a genuine saddle point on the closed shell potential surface, but one quite different in character to the alternative Woodward–Hoffmann geometrical process involving a single antarafacial component on one alkene. When the *anti* isomer **12** (Scheme 1) was studied, analogous results were obtained, leading to the product corresponding to the isomeric cyclooctatetraene **11**.

These PM3 transition structures were then re-optimised with *ab initio* methods. At the RHF/6-31G(d) level, **6** and **12** are computed as second order saddle points, with the genuine transition states (**2** and **8**) corresponding to the 4π-conrotatory opening of a side ring being lower in energy in all instances. With re-optimisation at the B3LYP density functional theory level, structures **6** and **12** again show only one imaginary frequency, except in specific instances of **6a** (R = NO_2) and **6f** (R = CF_3) where imaginary rotational modes of the substituent could not be eliminated. The geometry for one example is shown in Fig. 1. The trapezoidal angle ranges from 105.7° to 112.7°, with relatively little correlation with substituent.

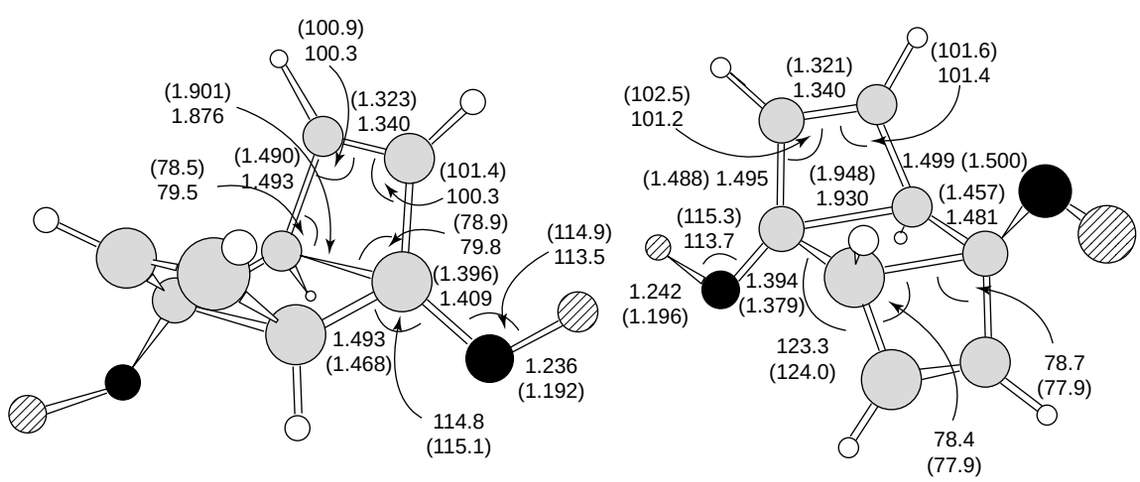

Fig. 1 B3LYP [RHF] calculated geometries (distances in Å and angles in degrees) for **6b** and **12b**. All Gaussian input geometries are linked to the Tables on the electronic version of this article.

Analysis of the frontier molecular orbital at the transition state in these systems shows greatly reduced electronic density on the carbon atom in the position β to the substituent (Fig. 2). Each forming σ bond is therefore associated predominantly with π electrons deriving from only one of the two alkene components, a process facilitated by the trapezoidal distortion of the geometry. This allows the creation of transition state saddle points in the potential surface to allow a ground state thermal reaction to proceed.

The energies computed for **6** are comparable to those obtained for transition states **2** (Table 1). Distinct geometries corresponding to **2b**, **2d** and **2e** could not be located in the potential surface at the B3LYP level, with geometry optimisation in these cases converging to the corresponding synchronous structure **6**. In contrast, the energy values for the transition states corresponding to the cycloelimination of the *trans*-isomer **12** are higher in energy than these obtained for the ring opening transformations of **8** in all the examples except **8e** (Table 2). This does imply that the kinetic behaviour of the *syn* series (proceeding *via* **6**) might be quite distinct from the *anti* series, which is still predicted to proceed *via* **8** and not **12**. Overall, the low energy barriers computed for **6d** and **6e** in particular suggest that the synchronous reaction pathway for these two systems in particular should be readily accessible under thermal conditions, and that experimental verification could be sought for this system.

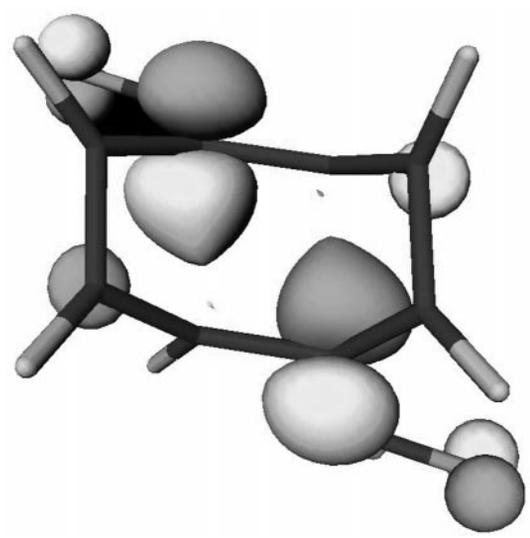

Fig. 2 Highest occupied molecular orbital at the transition state for **6b**. The sum of the squares of the coefficients at the carbon atom α to R is 0.348 and β is 0.015.

We offer two suggestions here. A classical experiment which can potentially distinguish between the kinetics of different types of bond cleavage would involve isotopic labelling of the reacting centres, with either ^{13}C or ^{2}H or both. If four centres are re-hybridising at the transition state, then the kinetic isotope effects induced can be distinguished from those induced by only two re-hybridising centres.[6] A more recently reported method by Zewail and co-workers[7] involves the application of laser-induced picosecond fluorescence spectroscopy. In principle, this allows estimates of the frequency of the transition normal mode. Our results consistently show that this mode has approximately twice the value (~600 cm^{-1}) for, *e.g.* synchronous transition state **6** than the asynchronous transition state **2**, a prediction which might be susceptible to experimental verification.

In light of these results, we decided to also study the potential surfaces for the parent $_{\sigma}2_s + _{\sigma}2_s$ cycloelimination of the corresponding substituted cyclobutanes **13** and **16** (Table 3, Scheme 2). A biradical mechanism for the $_{\pi}2_s + _{\pi}2_s$ cycloaddition–elimination of ethene had previously been computed

Table 1 Energies (activation barriers) and first two normal modes (cm^{-1}) for the stationary point structures in the *syn* series **2a**–**f** and **6a**–**f**

	PM3/Kcal mol^{-1}	ν_I/cm^{-1}	RHF/6-31G(d)/Hartree	ν_I/cm^{-1}	B3LYP/6-31G(d)/Hartree	ν_I/cm^{-1}
6a	137.81 (32.13)	−1462.4, 35.4	−714.30580 (44.76)	−729.9, −156.4	−718.453100 (29.04)	−581.0, −57.4
2a	136.44 (30.76)	−404.0, 24.0	−714.313751 (39.81)	−367.7, 73.9	−718.457735 (26.13)	−260.2, 33.4
6b	187.33 (34.77)	−1726.0, 55.4	−564.651556 (40.11)	−762.1, −177.0	−568.039409 (22.15)	−594.3, 71.9
2b	183.24 (30.68)	−465.4, 50.2	−564.654646 (38.17)	−251.1, 89.6	[a]	[a]
6c	91.54 (37.59)	−1931.4, 56.0	−532.826271 (38.94)	−760.5, −157.0	−536.094689 (29.34)	−610.7, 50.5
2c	85.66 (31.71)	−502.1, 67.7	−532.819760 (43.02)	−344.1, 77.2	−536.094701 (29.33)	−268.5, 75.1
6d	230.59 (30.98)	−1603.0, 38.2	−1178.10141 (35.47)	−755.6, −184.2	−1182.02562 (20.38)	−592.3, 59.7
2d	226.81 (27.20)	−378.3, 73.1	−1178.10270 (34.66)	−564.7, 55.8	[a]	[a]
6e	194.22 (20.81)	−1114.4, 65.9	−580.630131 (26.19)	−722.9, −94.7	−583.93349 (16.64)	−562.6, 77.5
2e	[a]		[a]	[a]	[a]	[a]
6f	−155.70 (39.55)	−2092.0, 11.5	−978.595931 (58.82)	−684.6, −188.8	−983.516719 (41.81)	−543.7, −111.8
2f	−163.15 (32.10)	−505.8, 22.4	−978.6152498 (46.70)	−502.25 42.49	−983.5428987 (25.38)	

[a] Structure **2** converges to **6** on optimisation.

Table 2 Energies (activation barriers) and first two normal modes (cm^{-1}) for the stationary point structures in the *anti* series **12a**–**f** and **8a**–**f**

	PM3/Kcal mol^{-1}	ν_I/cm^{-1}	RHF/6-31G(d)/Hartree	ν_I/cm^{-1}	B3LYP/6-31G(d)/Hartree	ν_I/cm^{-1}
12a	143.77 (41.32)	−1536.7, 12.1	−714.28286 (67.32)	−947.3, −199.5	−718.436029 (44.92)	−731.1, −50.0
8a	126.46 (24.01)	−632.3, 34.5	−714.312582 (48.64)	−422.3, 53.6	−718.4570768 (31.71)	−301.4, 51.9
12b	192.70 (42.58)	−2192.0, −24.0	−564.635383 (56.6)	−905.2, −227.4	−568.029491 (31.28)	−688.6, 64.8
8b	179.12 (29.00)	−614.9, 36.3	−564.652322 (45.96)	−415.7, 82.4	−568.0358131 (27.31)	−231.9, 84.1
12c	97.51 (37.59)	−1931.4, 56.0	−532.797939 (62.89)	−936.0, −230.2	−536.081062 (41.85)	−722.0, 13.2
8c	83.53 (34.56)	−1864.7, −52.9	−532.8200672 (42.83)	−457.3, 82.1	−536.0948409 (29.24)	−320.8, 79.6
12d	230.80 (31.71)	−505.4, 36.4	−1178.089342 (49.3)	−860.7, −265.2	−1182.017458 (29.29)	−688.2, 38.7
8d	225.01 (25.92)	−399.9, 36.0	−1178.0988767 (43.29)	−267.4, 55.4	−1182.021806 (26.56)	−220.4, 50.4
12e	196.00 (25.22)	−1185.3, 39.5	−580.620219 (37.99)	−827.8, −166.5	−583.926928 (22.88)	−619.7, 65.0
8e	[a]	[a]	−580.622577 (36.51)	−502.5, 53.5	[a]	[a]
12f	−149.02 (46.94)	−2731.2, 20.7	−978.571651 (78.12)	−879.1, −291.2	−983.498723 (56.64)	−699.9, −88.5
8f	−163.97 (31.99)	−491.8, 14.1	−978.614071 (51.50)	−573.7, 38.2	−983.530631 (36.61)	−392.7, 35.8

[a] Structure **8** converges to structure **12** on optimisation.

Table 3 Energies (activation barriers) and first two normal modes (cm^{-1}) for the stationary point structures in the series **14a–e** and **17a–e**

	PM3/Kcal mol^{-1}	ν_I/cm^{-1}	RHF/6-31G(d)/Hartree	ν_I/cm^{-1}	B3LYP/6-31G(d)/Hartree	ν_I/cm^{-1}
14a	70.78 (81.48)	−2736.1, 50.0	−562,887004 (98.75)	−1135.98, 68.15	−566.088886 (78.19)	−790.1, 68.6
14b	120.00 (87.07)	−3699.3, 46.2	−413.234724 (91.42)	−1062.9, 77.2	−415.684460 (62.38)	−700.4, 81.1
14c	23.09 (90.26)	−7597.7, 64.0	−381.395344 (93.80)	−1167.6, 63.7	−383.732769 (70.87)	−792.0, 64.0
14d	158.90 (81.09)	−3975.2, 34.1	−1026.686934 (82.02)	−948.5, 42.9	−1029.763774 (58.85)	−754.2, 47.4
14e	121.57 (71.34)	−1621.7, 64.8	−429.2237306 (67.68)	−879.6, 86.8	−431.585576 (46.89)	−563.8, 88.4
17a	69.44 (80.60)	−2602.0, 37.6	−562.894627 (94.18)	1097.4, 67.4	−566.095655 (73.94)	−747.6, 63.7
17b	119.72 (86.90)	−3687.4, 49.4	−413.235822 (88.93)	−1067.2, 73.8	−415.685351 (61.73)	−696.3, 70.0
17c	23.06 (90.23)	−7870.0, 49.6	−381.395085 (94.92)	−1174.7, 65.3	−383.732169 (72.37)	−798.8, 57.0
17d	159.10 (81.30)	−4133.4, 36.4	−1026.686318 (80.86)	−959.6, 42.0	−1029.669067 (58.76)	−756.4, 34.5
17e	120.61 (70.53)	−1670.8, 51.7	−429.224035 (67.07)	−890.5, 62.8	−431.586326	−561.3, 68.9

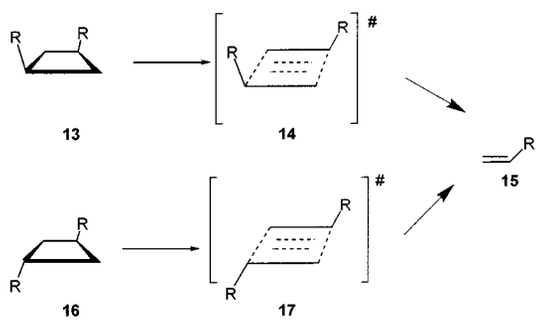

Scheme 2

for this process by Bernardi *et al.*[8] and by Olivella *et al.*[9] Antarafacial geometries ($_{\pi}2_s + {}_{\pi}2_a$) were found by Bernardi *et al.* to correspond to second order saddle points at MCSCF levels of theory, distorting to biradical-like transition states. Higher cycloaddition homologues such as $_{\pi}4_s + {}_{\pi}4_a$ and $_{\pi}6_s + {}_{\pi}6_a$ cycloadditions[10] were similarly found to be second-order saddle points at RHF levels of theory. The characteristic feature of all these previous studies is that no genuine transition states could be located by the single-determinantal closed shell RHF method, and only the use of multi-configuration open-shell (MCSCF) methods led to any first-order saddle points. To our knowledge an alternative trapezoidal pathway for cycloaddition reactions has not hitherto been discussed or characterised.

In our case, the single determinantal RHF method applied to the structures **14a–f** and **17a–f** did indeed result in characterisable transition states (Table 3), the most noticeable features of which are again a strongly trapezoidal C_{2h} geometry, but in this case associated also with thermally unrealistic high energy barriers. These trapezoidal characteristic angles (ranging from 106.0° to 115.8°) are more pronounced for **14a–f** and **17a–f** than for **6a–f** and **12a–f** because of the absence of the additional geometrical constraints induced by the additional rings in the latter. Nevertheless, these results do establish that the qualitative change in the potential energy surface for the $_{\pi}2_s + {}_{\pi}2_s$ cycloaddition–elimination reaction was not fundamentally due to the characteristics present in **6** or **12**, such as ring strain or torquoselectivity effects on the conrotatory electrocyclic ring opening.[11] Rather, it is the distortions in the wavefunctions at the transition state due to the presence of the electron-withdrawing substituents that create a thermally allowed reaction mode. A simple analogy is that the presence of strongly electron-withdrawing substituents effectively reduces the electron count for the reacting system from four electrons to (in the limit) two, and that the trapezoidal shapes are the result of π-allyl-cation like structures.

Conclusions

We have established that at PM3 or B3LYP/6-31G(d) levels of theory, the potential energy surface for a simple pericyclic reaction such as a $_{\pi}2_s + {}_{\pi}2_s$ cycloaddition–elimination can be qualitatively modified by pairs of electron-withdrawing substituents, to allow a geometric alternative to the Woodward–Hoffmann antarafacial distortion required for a thermal reaction. Such a trapezoidal distortion allows a fully synchronous transition state **6** for the transformation of species **1** to **5** to become the predicted favoured route with substituents such as R = NO, CHS or CF (carbene). We are currently investigating whether a similar re-engineering of the potential energy surface might be possible for other related examples of pericyclic reactions.

Acknowledgements

We thank the Spanish Ministerio de Educación y Cultura for a postdoctoral fellowship (to C. C.).

References

1 C. Conesa and H. S. Rzepa, *J. Chem. Soc.*, *Perkin Trans. 2*, 1998, 857.
2 J. J. P. Stewart, MOPAC, *Quantum Chemistry Program Exchange*, University of Indiana, Bloomington, USA, Program 455.
3 Gaussian program systems available from Gaussian Inc., 4415 Fifth Avenue, Pittsburgh, PA, USA.
4 H. B. Schlegel, *J. Comput. Chem.*, 1982, **3**, 214.
5 C. Peng and H. B. Schlegel, *Isr. J. Chem.*, 1993, **33**, 449.
6 M. J. S. Dewar, S. Olivella and H. S. Rzepa, *J. Am. Chem. Soc.*, 1978, **100**, 5650.
7 B. A. Horn, J. L. Herek and A. H. Zewail, *J. Am. Chem. Soc.*, 1996, **118**, 8755.
8 F. Bernardi, A. Bottoni, M. A. Robb, H. B. Schlegel and G. Tonachini, *J. Am. Chem. Soc.*, 1985, **107**, 2260; F. Bernardi, A. Bottoni, M. A. Robb and A. Venturini, *ibid.*, 1990, **112**, 2106.
9 J. M. Bofill, J. Gomez and S. Olivella, *J. Mol. Struct.* (*THEOCHEM*), 1988, **63**, 285.
10 H. S. Rzepa and W. A. Wylie, *J. Chem. Soc.*, *Perkin Trans. 2*, 1991, 939; H. S. Rzepa, *ibid.*, 1989, 2115.
11 W. R. Dolbier, H. Koroniak, D. J. Burton, A. R. Bailey, G. S. Shaw and S. W. Hansen, *J. Am. Chem. Soc.*, 1984, **106**, 1871; N. D. Epiotis, *J. Mol. Struct.* (*THEOCHEM*), 1990, **66**, 225; S. Niwayama and K. N. Houk, *Tetrahedron Lett.*, 1992, **33**, 883.

Paper 8/05668D